caution. If in Fig. 1 the radius of the circle centered at the origin is increased such that it is nominally tangent to the line between w_1 and w_2, it then appears that two possible minima for F will exist, especially if σ_3 is large. These correspond approximately to the points of intersection of the circles centered at w_1 and w_2. Alternatively, if the radius of the circle centered at the origin and σ_3 are both very small, and if the circles centered at w_1 and w_2 intersect at the origin, then the origin may actually correspond to a (local) maximum of F, while if one traverses the perimeter of the circle centered at the origin one will alternately encounter a series of four minima and four saddle points. (These correspond to the set of nine possible roots for a pair of simultaneous cubic equations.)

Fortunately, however, considerations of these types tend to be somewhat remote from the projected applications. Further study of this topic is in progress and will be reported in due time.

References

[1] G. F. Engen, "The six-port reflectometer: an alternative network analyzer," *IEEE Trans. Microwave Theory Tech.*, vol. MTT-25, pp. 1075–1079, Dec. 1977.

[2] C. A. Hoer, "A network analyzer incorporating two six-port reflectometers," *IEEE Trans. Microwave Theory Tech.*, vol. MTT-25, pp. 1070–1074, Dec. 1977.

[3] G. F. Engen and C. A. Hoer, "Thru-reflect-line: an improved technique for calibrating the dual six-port automatic network analyzer," *IEEE Trans. Microwave Theory Tech.*, vol. MTT-27, pp. 987–993, Dec. 1979.

[4] G. F. Engen, "Calibrating the six-port reflectometer by means of sliding terminations," *IEEE Trans. Microwave Theory Tech.*, vol. MTT-26, pp. 951–957, Dec. 1978.

Circular-Electric Mode Waveguide Couplers and Junctions for Use in Gyrotron Traveling-Wave Amplifiers

LARRY R. BARNETT, MEMBER, IEEE, J. MARK BAIRD, MEMBER, IEEE, ARNE W. FLIFLET, AND VICTOR L. GRANATSTEIN

Abstract—**Recent gyrotron traveling-wave amplifier experiments in the TE_{01}° mode have led to the developing of 2-port and 4-port devices potentially useful as input couplers, severs, and beam–RF separators for collector designs. The couplers are moderately wide-band, have high transmission efficiencies, and low reflection coefficients. In addition, they are relatively easy to construct. We present analytical and experimental results.**

Introduction

RECENT EXPERIMENTS with a gyrotron traveling-wave amplifier operating in the TE_{01} circular waveguide mode [1] have spurred interest in developing circular-electric mode components. The recently reported amplifier experiments [1], which operate at 35 GHz, attained 30-dB gain in a single stage with 10-kW output. The useful small-signal bandwidth was on the order of 1 GHz. The input coupler in this amplifier consisted of a TE_{01} coaxial mode to TE_{01} circular mode junction. The TE_{01} coaxial mode was produced from TE_{10} rectangular waveguide by a coaxial sector waveguide taper. A taper study is described in the companion paper [2]. The work has expanded beyond the original coupler development and has resulted in devices potentially useful in circular-electric mode amplifiers and oscillators or designs with circular-electric outputs [3], [4], [8].

Manuscript received May 20, 1980; revised September 18, 1980. This work was supported by the Naval Electronics System Command, Washington, DC, under Task XF 54 581 007.

L. R. Barnett, J. M. Baird, and A. W. Fliflet are with B-K Dynamics, Inc., Rockville, MD, 20850.

V. L. Granatstein is with the Naval Research Laboratory, Washington, DC 20375.

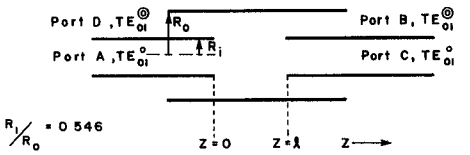

Fig. 1. Marcatili 4-port hybrid coupler.

Background

The initial design for the 2-port input coupler was derived from the Marcatili 4-port circular hybrid junction [5], [6]. The 4-port hybrid is shown in Fig. 1. An input at

0018-9480/80/1200-1477$00.75 ©1980 IEEE

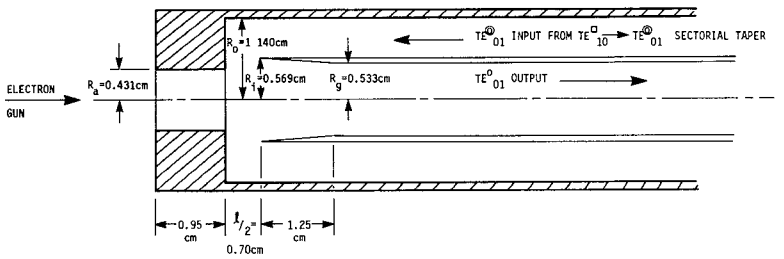

Fig. 2. The input coupler, $TE^{\circledcirc}_{01}$ to TE°_{01}, for the gyrotron traveling-wave amplifier.

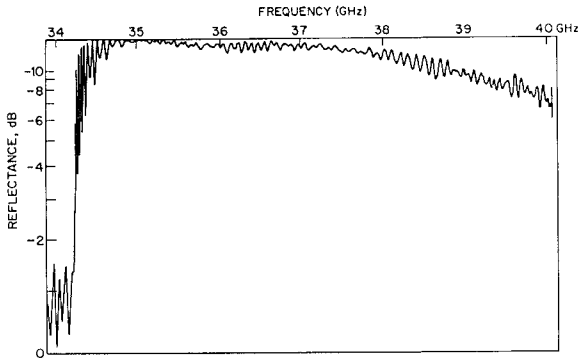

Fig. 3. Reflection measurement of the input coupler of Fig. 2 as seen from the TE°_{01} output port with an absorbed load in the $TE^{\circledcirc}_{01}$ input port.

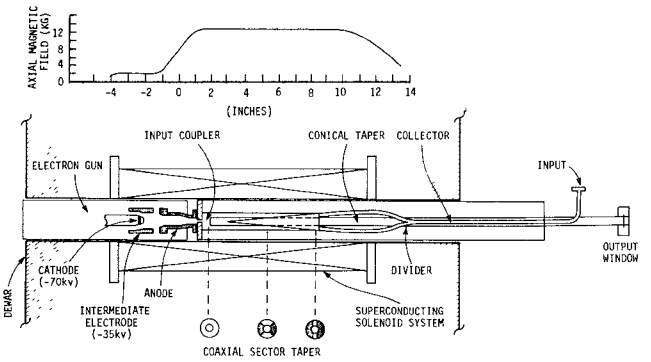

Fig. 4. The experimental gyrotron traveling-wave amplifier.

port A excites TE°_{01} and TE°_{02} propagating modes at $z=0$ in the gap region. The outer guide radius R_o is small enough to be cut off to circular-electric modes above TE°_{02} and therefore the excited TE°_{03} and above modes are evanescent. R_1 is placed at the TE°_{02} electric field null. when l is adjusted such that

$$\left(\frac{2\pi}{\lambda_{g01}}-\frac{2\pi}{\lambda_{g02}}\right)l \cong (2n-1)\pi \tag{1}$$

where λ_{g01} and λ_{g02} are the waveguide wavelengths and n is an integer, then the TE°_{01} and TE°_{02} modes are in the phase relationship to couple most of the energy to port B in the $TE^{\circledcirc}_{01}$ mode. When

$$\left(\frac{2\pi}{\lambda_{g01}}-\frac{2\pi}{\lambda_{g02}}\right)l \cong 2n\pi \tag{2}$$

then most of the energy is coupled to port C in TE°_{01}.

Equations (1) and (2) do not take into account the small phase shifts introduced by evanescent fields and the exact adjustment of l is easily accomplished by a sliding-tube arrangement. Power division can be accomplished by in-between adjustments of the gap length l. This hybrid has good bandwidth (>20 percent) and a transmission loss at the center frequency of ~0.3 dB [5]. The device, as is, would make an effective sever for traveling-wave amplifiers. Marcatili made no further improvement [5] in the hybrid. We now show that the ratio of the wall radii R_i/R_o can be adjusted to obtain certain advantages. We extend the concepts to other uses and a more advanced coupling scheme using three modes.

The input coupler used in the 35-GHz gyrotron traveling-wave amplifier [1] was made by placing a plane reflector at $z=l/2$ to make a 2-port junction between port A in TE°_{01} and port D in TE°_{01}. A sectorial waveguide taper from TE_{10} rectangular waveguide produced a TE_{01} coaxial input. A small hole in the reflector allowed entrance of the electron beam for interaction with the TE°_{01} mode in the central circular guide. The input coupler is shown in Fig. 2 and its measured reflection properties in Fig. 3. The sharp rise in reflection at 34.3 GHz corresponds to the cutoff frequency of the 0.533 radius output waveguide. The experimental gyro-TWA [1] in which it was used is shown in Fig. 4.

The devices thus far described utilize two propagating modes and will be referred to as 2-mode devices. Calculations and experiments show that 3-mode coupling is possible and such 3-mode devices have advantages over 2-mode devices in certain applications.

Coupling Theory

The coupling coefficients can be found by solving for the mode voltages of the modes, given the boundary conditions and transverse electric field (or an approximate field) in the waveguide at the junction [7]. In this case:

$$\boldsymbol{E}_t = \Sigma_i (\boldsymbol{e}_i^e V_i^e + \boldsymbol{e}_i^m V_i^m) \tag{3}$$

where E_t is the transverse electric field at the junction (for instance, the TE°_{01} mode at $z=0$ in Fig. 1), e_i^e are the TE mode vectors, e_i^m are the TM mode vectors, and V_i^e and V_i^m are TE and TM mode voltages, respectively. By the

orthogonality of the mode vectors then

$$\int_s\int \boldsymbol{E}_t \cdot \boldsymbol{e}_i^e \, ds = V_i^e$$

$$\int_s\int \boldsymbol{E}_t \cdot \boldsymbol{e}_i^m \, ds = V_i^m. \tag{4}$$

In this circular symmetrical geometry with TE_{0n} excitation TM modes will not be excited. The superscript e will then be dropped with the understanding that TE modes are being represented. If the mode vectors are normalized in their respective regions

$$\int_s\int \boldsymbol{e}_i \cdot \boldsymbol{e}_i \, ds = 1 \tag{5}$$

then

$$\int_s\int \boldsymbol{e}_j \cdot \boldsymbol{e}_i \, ds = C_j^i \tag{6}$$

defines the voltage coupling coefficient for excitation of e_i by e_j where e_j is the exciting mode and e_i the output mode at the junction. Note that $C_j^i = C_i^j$.

The mode vectors are given by

$$\boldsymbol{e} = \hat{u}_z \times \nabla_t \psi \tag{7}$$

where for the circular electric modes

$$\psi_{0n}^{\circ} \propto J_0\left(\frac{x'_{0n}\rho}{R_o}\right) e^{-jk_{0n}z} \tag{8}$$

$$\psi_{01}^{\circledcirc} \propto \left\{N_0'(k\rho R_i)J_0(k_\rho \rho) - J_0'(k_\rho R_i)N_0(k_\rho \rho)\right\} e^{-jk_{01}z} \tag{9}$$

where k_ρ is the first root of

$$J_0'(k_\rho R_i)N_0'(k_\rho R_o) - N_0'(k_\rho R_i)J_0'(k_\rho R_o) = 0. \tag{10}$$

Using the above expressions, we find that the coupling coefficients to the first few TE_{0n}° modes at $z=0$ when excited by a TE_{01}° input at port A in Fig. 1 are

$$C_{01}^{01} = \frac{2}{J_2^2(x'_{01})R_i R_o}\int_0^{R_i} J_1\left(\frac{x'_{01}}{R_i}\rho\right) J_1\left(\frac{x'_{01}}{R_o}\rho\right)\rho \, d\rho \tag{11}$$

$$C_{01}^{02} = \frac{2}{J_2(x'_{01})J_2(x'_{02})R_i R_o}\int_0^{R_i} J_1\left(\frac{x'_{01}}{R_i}\rho\right) J_1\left(\frac{x'_{02}}{R_o}\rho\right)\rho \, d\rho \tag{12}$$

$$C_{01}^{03} = \frac{2}{J_2(x'_{01})J_2(x'_{03})R_i R_o}\int_0^{R_i} J_1\left(\frac{x'_{01}}{R_i}\rho\right) J_1\left(\frac{x'_{03}}{R_o}\rho\right)\rho \, d\rho. \tag{13}$$

At $R_i/R_o = x'_{01}/x'_{02}$, (9) reduces to

$$\psi_{01}^{\circledcirc} \propto J_0\left(\frac{x'_{02}}{R_o}\rho\right) e^{-jk_{01}z} \tag{14}$$

and coupling equations similar to (11)–(13) are obtained. Since the rest of this paper will be concerned only with coupling coefficients to TE_{01}° exciting modes then the subscripts will be dropped, i.e., C_{01}^{01} will be represented by C^{01}, C_{01}^{02} by C^{02}, etc.

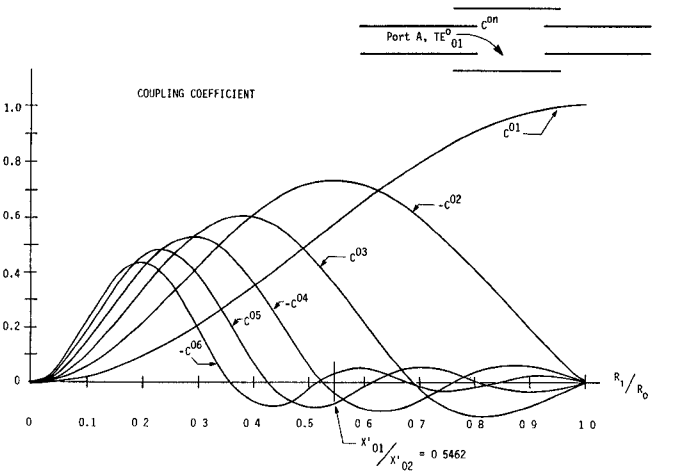

Fig. 5. Coupling coefficients from the TE_{01}° input to port A of the TE_{0n}° modes in the gap as a function of the ratio of the waveguide radii.

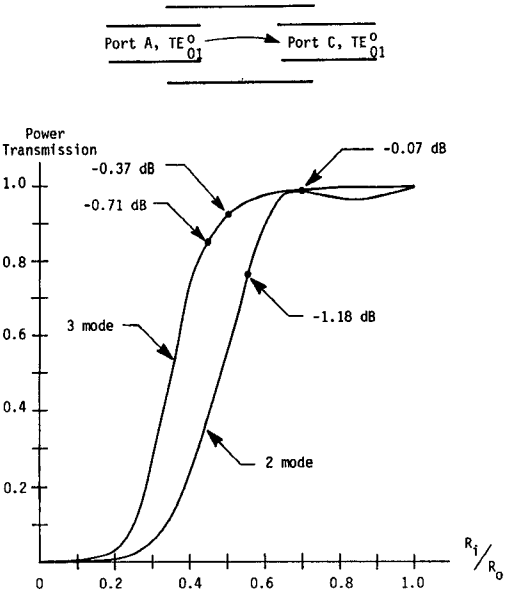

Fig. 6. Power transmission from port A to port C for 2-mode coupling and 3-mode coupling as a function of the ratio of the waveguide radii.

Fig. 5 shows plots of the coupling coefficients to the first six TE_{0n}° modes in the gap region as functions of R_i/R_o as excited by a TE_{0n}° input at port A. Suppose the gap l is adjusted for (2). Then the voltage coupling from port A to the output, port C, for 2-mode propagation can readily be calculated by

$$C_{AC} \cong (C^{01})^2 + (C^{02})^2. \tag{15}$$

Calculating the coupling from a coaxial port to the modes and adjusting l for (1) the coupling from port A to port B can be obtained.

Fig. 6 shows the power transmission from port A to port C for 2-mode coupling as a function of R_i/R_o. Three-mode coupling is accomplished by making the radius of the gap region above TE_{03}° cutoff. However, 3-mode coupling is successful only for specific values of R_o in order

to obtain the proper relative phasing between the mode vectors.

The proper phasing occurs when

$$\Delta k = \frac{2\pi}{l} \text{ or a multiple of } \frac{2\pi}{l} \tag{16}$$

for all modes where Δk is the difference between each of the propagation constants i.e., $k_{01}-k_{02}$, $k_{02}-k_{03}$, $k_{01}-k_{03}$.

The set of equations (16) gives

$$\left(1-\frac{f_{c02}^2}{f^2}\right)^{1/2}-\left(1-\frac{f_{c03}^2}{f^2}\right)^{1/2} = m\left[\left(1-\frac{f_{c01}^2}{f^2}\right)^{1/2}-\left(1-\frac{f_{c02}^2}{f^2}\right)^{1/2}\right] \tag{17}$$

where f_{c0n} is the cutoff frequency of the TE_{0n}° modes in the gap region and m is an integer. Equation (17) can be used to find frequencies satisfying (16) as the radius R_o is held constant (and hence the cutoff frequencies). Then an l is found as by

$$l = \frac{2\pi n}{k_{01}-k_{02}} \tag{18}$$

when n is any integer. Once a design is chosen (note that there is no unique solution) then the dimensions are scaled to the proper operating frequency. The 3-mode coupling shown in Fig. 6 is for $m=2$ and the smallest solution for R_o (still cutoff to TE_{04}°). Note that the 3-mode coupler transmission is more efficient than the 2-mode coupling, especially for $R_i/R_o<0.6$. At $R_i/R_o=0.69$ the coupling loss of both is the same, 0.07 dB. At this point, the coupling to the TE_{03}° mode goes to zero. Not only is the 3-mode coupler generally more efficient, but it is physically much larger than the 2-mode coupler. In the 35-GHz experimental couplers to be described, $R_o=1.181$ cm for the 2-mode and $R_o=1.687$ cm for the 3-mode solution given above. The gap length increased from 2.76 cm for the 2-mode to 6.71 cm for the 3-mode case. The increase in size is an advantage for using the outer wall as a beam collector or for a beam–RF separator which requires room for the beam to exit out of port B as guided by magnetic field lines. In this application, we would also want R_i/R_o to be small and still maintain efficient coupling to port C. The 3-mode coupling is more efficient at the smaller ratios. Also, one could set $R_i/R_o=0.69$ and utilize the TE_{04}° mode as the third mode making the overall size even larger. Possibly even larger sizes could be made since coupling to the TE_{05}° and higher modes is -26 dB or less and may not seriously impair performance.

We have performed experiments measuring the 2-mode coupling just described. Reflection- and transmission-loss measurements were made by conventional directional couplers and power sensors in standard *Ka*-band rectangular waveguide and using Hitachi Denshi, Ltd. tapered mode transitions, model R6414, together with TE_{01}° mode filters, model R9308, to convert from $TE_{10}^{\square}$ to TE_{01}°. Conical sections were used to taper from the mode transitions

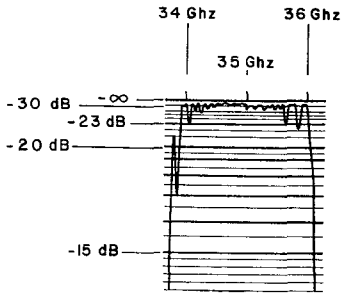

Fig. 7. Reflection measurement from port A of the 3-mode coupler of Fig. 6 with absorber loads in the other ports.

diameter, 1.60 cm, to the required input or output diameter of the experiment. The reflection measurements presented, therefore, include all reflections from the mode transitions and conical tapers as well as the experiments. The transmission loss of each mode transition with one mode filter was 0.5 dB. The transmission loss through the experiment was measured by comparing the power transmitted with the appropriate gap length to the transmitted power with the gap length set to zero.

In both couplers $R_i/R_o=x'_{01}/x'_{02}=0.546$. The midband measured loss at 35 to 36 GHz for the 2-mode coupler is 0.2 to 0.4 dB. The transmission bandwidth edges for 1-dB loss were ~34.0 to 40.0 GHz. The reflection coefficient from port A was ~ -15 dB from 34.5 to 40.0 GHz and much lower at midband. Fig. 7 shows the measured reflection coefficient of the 3-mode coupler. The 3-mode coupler has an almost rectangular window about 2 GHz wide centered at 35 GHz with a reflection coefficient of -23 dB or less at the band edges and going down to -30 dB or less at midband. The measured transmission loss was on the order of 0.05 dB over the 2-GHz band. The 2-mode coupler could be tuned to optimum performance at other center frequencies by varying the gap length l. As expected, the 3-mode coupler could not be tuned and only worked well near its designed frequency of 35 GHz.

Some discrepancy is observed between calculations and experiments. The calculation of coupling for the 2-mode hybrid coupler of Fig. 6 at $R_i/R_o=0.546$ indicates about 1-dB loss should occur. Experiments by both Marcatili [5] and for this paper indicate an ~0.3-dB or less transmission loss occurs. The coupling coefficients predicted in this paper were calculated on the basis that all the modes with significant coupling were below cutoff. The 2-mode coupling of Fig. 6 was then calculated as if the TE_{03} and higher mode energy was being wasted, when in reality, the existence of coupling to evanescent modes results in modified coupling to the propagating modes and output power is coupled to all the ports instead of the desired one port. Fig. 6 is then most accurate when coupling to evanescent modes is small, i.e., when $R_i/R_o \gtrsim 0.64$ in the 2-mode coupler and $R_i/R_o \gtrsim 0.48$ in the 3-mode coupling, etc. A fuller theory is in progress.

One interesting application for a beam–RF separator would be to start with large R_o (well above TE_{03}° cutoff

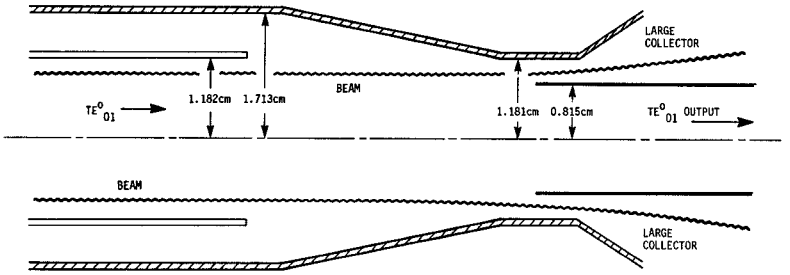

Fig. 8. A suggested beam–RF separator.

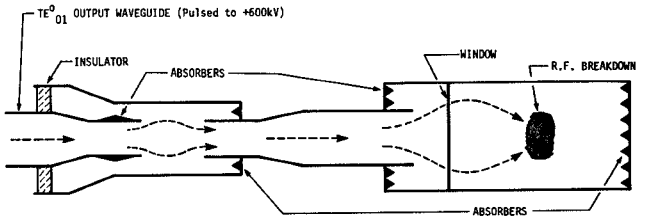

Fig. 9. Schematic of the proposed output waveguide system for the NRL hybrid inverted coaxial magnetron.

but below TE°_{04} cutoff) at $z=0$ for $R_i/R_o=0.69$ and taper down to below TE°_{03} cutoff at $z=l$. The TE°_{03} is not excited at $R_i/R_o=0.69$ and hence no loss of match will occur. The electron beam could, therefore, travel straight through the device into a large collector. Fig. 8 shows a possible design (untested as yet) for operation at 35 GHz. The taper must not introduce significant mode conversion. Tuning could be accomplished with a sliding tube arrangement in the straight sections.

Other uses of these couplers are being planned at NRL for the 3.2-GHz gigawatt level hybrid inverted coaxial magnetron [8] which has a TE°_{01} output. The 4-port coupler is readily insulated to high voltage between the input and output ports and this will be used for isolation of the 600-kV anode pulse from the output waveguide. Variable power division is possible as well. At present, an inductive helical winding isolates the 55-ns anode pulse and passes the TE°_{01} output, but longer pulse lengths are desired. The magnetron will be used for RF breakdown studies and the breakdown chamber is planned to be a version of the 3-mode coupler without the output waveguide. Breakdown should take place near $z=l$ since the field pattern at that point is essentially an image of the TE°_{01} mode at the input waveguide. The window will be placed at a low-field point. A simplified tentative schematic of the system is shown in Fig. 9. The TE°_{01} output waveguide labeled in Fig. 9 is the output waveguide of the magnetron. The arrows only symbolically represent the flow of microwave energy. Detailed field patterns can be found from (3).

Conclusion

We conclude by noting that, by the analysis and experiments performed wide-band and efficient circular-electric mode coupling schemes can be used for several applications which utilize circular TE modes. In this summary we have only introduced a few possible applications but we anticipate that others will become apparent as research continues.

References

[1] L. R. Barnett, K. R. Chu, J. M. Baird, V. L. Granatstein, and A. T. Brobot, "Gain, saturation, and bandwidth measurements of the NRL gyrotron traveling wave amplifier," in *IEEE Int. Electron Devices Meet. (IEDM) Tech. Dig.*, pp. 164–167, 1979.

[2] A. W. Fliflet, L. R. Barnett, and J. M. Baird, "Mode coupling and power transfer in a coaxial sector waveguide with a sector angle taper," in *IEEE MTT-S Int. Microwave Symp. Dig.*, pp. 93–95, 1980; also this issue, pp. 1482–1486.

[3] J. M. Baird, "Survey of fast wave tube developments," in *IEEE Int. Electron Devices Meet. (IEDM) Tech. Dig.*, pp. 156–163, 1979.

[4] M. E. Read, R. M. Gilgenback, A. J. Dudas, R. Lucey, K. R. Chu, and V. L. Granatstein, "Operating characteristics of a 35 GHz gyromonotron," in *IEEE Int. Electron Devices Meet. (IEDM) Tech. Dig.*, pp. 172–174, 1979.

[5] E. A. J. Marcatili, "A circular-electric hybrid junction and some channel-dropping filters," *Bell Syst. Tech. J.*, vol. 40, pp. 185–196, Jan. 1961.

[6] E. A. J. Marcatili, U.S. Patent 2 969 670, Nov. 1960.

[7] R. F. Harrington, *Time Harmonic Electromagnetic Fields*. New York: McGraw-Hill, 1961, ch. 8.

[8] W. M. Black, R. K. Parker, R. Tobin, G. Farney, M. Herndon, and V. L. Granatstein, "A hybrid inverted coaxial magnetron to generate gigawatt levels of pulsed microwave power," in *IEEE Int. Electron Devices Meet. (IEDM) Tech. Dig.*, pp. 175–178, 1979.